

## Rutheniumethynyl-triarylamine mixed-valence conjugated system: syntheses, (spectro-)electrochemistry, and theoretical calculations

YA-Ping Ou, Yuxuan Hu, Meng Xu, Aihui Wang & Sheng Hua Liu

To cite this article: YA-Ping Ou, Yuxuan Hu, Meng Xu, Aihui Wang & Sheng Hua Liu (2019): Rutheniumethynyl-triarylamine mixed-valence conjugated system: syntheses, (spectro-)electrochemistry, and theoretical calculations, Journal of Coordination Chemistry, DOI: [10.1080/00958972.2019.1695125](https://doi.org/10.1080/00958972.2019.1695125)

To link to this article: <https://doi.org/10.1080/00958972.2019.1695125>

 View supplementary material 

 Published online: 28 Nov 2019.

 Submit your article to this journal 

 Article views: 3

 View related articles 

 View Crossmark data 



# Rutheniumethynyl-triarylamine mixed-valence conjugated system: syntheses, (spectro-)electrochemistry, and theoretical calculations

YA-Ping Ou<sup>a</sup>, Yuxuan Hu<sup>b</sup>, Meng Xu<sup>b</sup>, Aihui Wang<sup>a</sup> and Sheng Hua Liu<sup>b</sup>

<sup>a</sup>Key Laboratory of Functional Metal-Organic Compounds of Hunan Province, Key Laboratory of Functional Organometallic Materials of Hunan Province College, College of Chemistry and Material Science, Hengyang Normal University, Hengyang, P.R. China; <sup>b</sup>Key Laboratory of Pesticide and Chemical Biology, Ministry of Education, College of Chemistry, Central China Normal University, Wuhan, P.R. China

## ABSTRACT

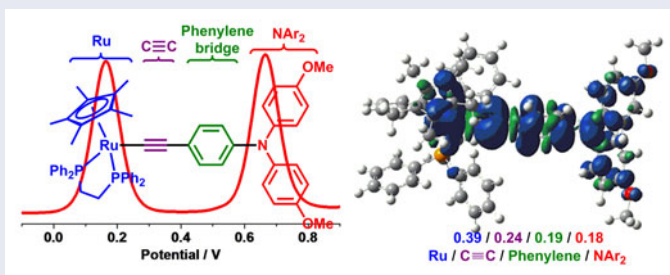
We describe the synthesis and characterization of triarylamine ethynyl ruthenium conjugate (4-OMeC<sub>6</sub>H<sub>4</sub>)<sub>2</sub>N-{C<sub>6</sub>H<sub>4</sub>-4-C≡C-RuCp\* (dppe)}, **3**. Its electronic and spectroscopy properties are investigated by anodic voltammetry, IR and UV-vis-NIR spectroelectrochemistry, and density functional theory (DFT) calculations. Results indicate that **3** undergoes two well-defined single-electron redox processes and that the Ru<sup>II/III</sup> process occurs prior to the N<sup>0/+</sup> process as supported by IR spectra  $\nu(\text{C}\equiv\text{C})$  band changes from **3** to **3**<sup>+</sup> ( $\Delta\nu = 129 \text{ cm}^{-1}$ ) and spin-density distribution calculations of **3**<sup>+</sup>. TDDFT calculations further reveal the NIR characteristic bands of singly oxidized **3**<sup>+</sup> from experimental spectroscopic absorptions, and we observe NAr<sub>2</sub>→Ru charge transfer mixed with Ru-C≡C→phenyl bridge charge-transfer.

## ARTICLE HISTORY

Received 18 July 2019  
Accepted 6 November 2019

## KEYWORDS

Triarylamine; ruthenium; anodic voltammetry; spectroelectrochemistry; DFT calculations



## 1. Introduction

Organic and organometallic mixed-valence (MV) compounds attract wide research interest from experimentalists and theorists because they serve as models of molecule wires to evaluate electron-transfer processes [1–3]. These models usually comprise of

CONTACT YA-Ping Ou ouyaping@Hynu.edu.cn; Sheng Hua Liu Chshliu@Mail.ccnu.edu.cn

Supplemental data for this article is available online at <https://doi.org/10.1080/00958972.2019.1695125>.

© 2019 Informa UK Limited, trading as Taylor & Francis Group

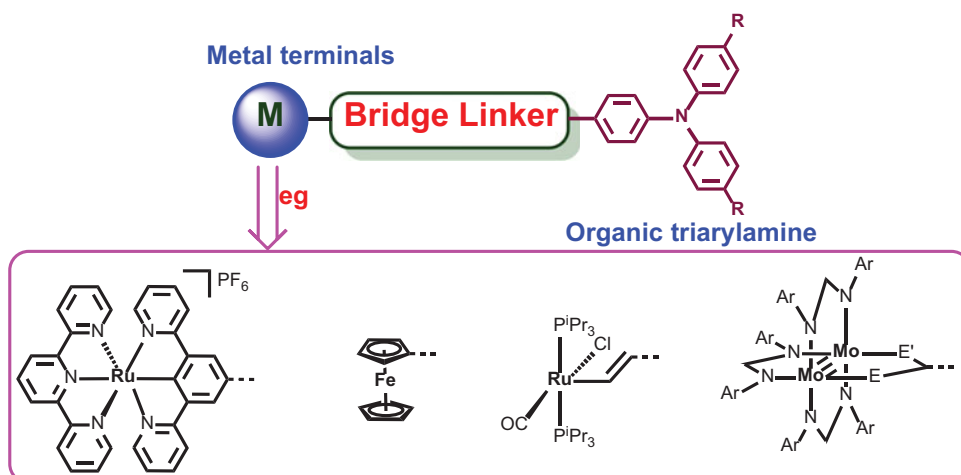


**Chart 1.** Organic-inorganic hybrid MV systems with triarylamine and transition metals as redox-active terminals.

conjugated bridge chains and redox-active end groups. Most research has focused on building up symmetrical (with two degenerate redox centers) model structures and deeply investigating the influence of the structural properties of the bridge spacer (length, degree of conjugation, and electronic properties) [4–7] or the nature of redox centers [3, 8–12] on electronic coupling. Their characteristic near-infrared (NIR) intervalence charge-transfer (IVCT) transition absorptions generated from *in situ* spectroelectrochemical experiments provided useful parameters (reorganization energy ( $\lambda$ ), electronic coupling parameter ( $V_{ab}$ ), and degree of charge delocalization) to classify MV systems [1–3, 13–15].

However, the types of bridged chain units and redox-active end groups are limited. Thus far, symmetrical organic or inorganic MV complexes with conjugated bridge units such as conjugated polyene [11], polyacetylene [16, 17], polycyclic aromatic hydrocarbons [4, 18, 19], or hetero-aromatic hydrocarbons [10, 20], as well as redox-active end groups such as iron [8, 21], ruthenium [11, 12, 16, 18, 22, 23], osmium [24], or organic triarylamine [25, 26] and tetrathiafulvalene [27] have been reported. Thus, to expand further the variety of MV species and explore novel electronic properties, scientists have begun to construct asymmetric redox-active terminal compounds connected by conjugated bridge linkers [28].

As an important member of asymmetric redox-active end-group compounds, organic-inorganic hybrid MV systems have become an important research topic for scientists [29–32]. Triarylamine and its derivatives have excellent electrical, optical, and redox properties and are thus widely used in photoelectric materials and solar cells [33, 34], especially as the end group in organic MV systems [35, 36]. Many research groups have reported several characteristic organic-inorganic MV systems with triarylamine and transition metals as redox-active terminals (Chart 1) [31, 37–42]. For example, Winter *et al.* [39] described the synthesis and characterization of triarylamine-vinylruthenium conjugate **1** and investigated its charge and spin delocalization and substituent effects. Zhong *et al.* [40] demonstrated the electronic coupling and

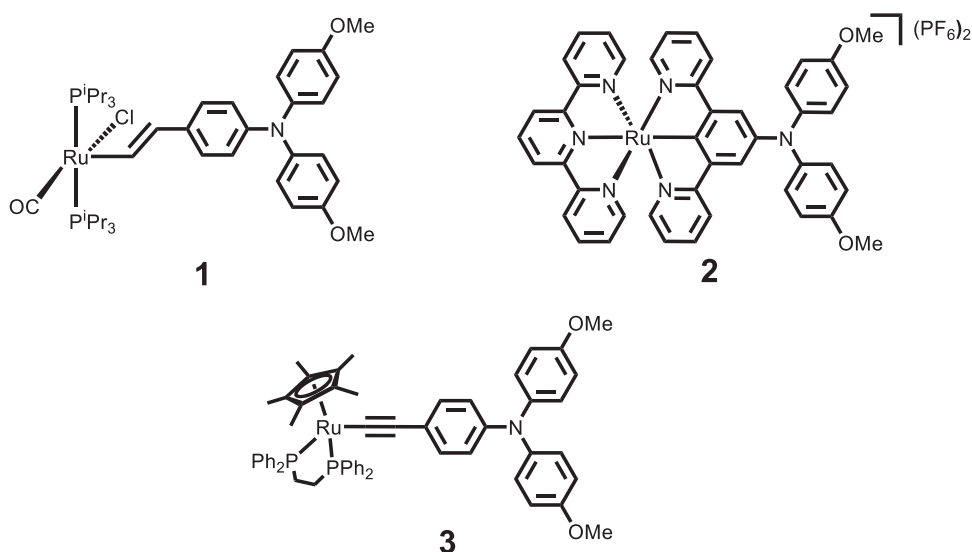


**Figure 1.** Ruthenium-triarylamine conjugated systems 1–3.

charge transfer direction of cyclometalated ruthenium-triarylamine complex **2**. However, the possible linkage of ruthenium-ethynyl to triarylamine to construct such a system is still rarely reported [43]. Accordingly, in the present work, we designed and synthesized complex **3** (Figure 1) and then systematically studied its electron coupling and delocalization characteristics.

## 2. Experimental

### 2.1. Materials and methods

All manipulations were carried out at room temperature under a dry nitrogen atmosphere using standard Schlenk techniques, unless otherwise stated. Solvents were pre-dried, distilled, and degassed prior to use, except those for spectroscopic measurements, which were of spectroscopic grade. The main reagents *p*-bromoaniline, *p*-iodoanisole, 1,10-phenanthroline, CuI, KOH trimethylsilylacetylene and  $[\text{Pd}(\text{PPh}_3)_4]$  were commercially available. The starting materials  $[\text{RuCp}^*\text{Cl}(\text{dppe})]$  [44] and intermediate compounds **3b** and **3c** [45] were prepared by the literature methods.

$^1\text{H}$ ,  $^{13}\text{C}$ , and  $^{31}\text{P}$  NMR spectra were collected on a Varian Mercury Plus 500 spectrometer (500 MHz).  $^1\text{H}$  and  $^{13}\text{C}$  NMR chemical shifts are relative to TMS and  $^{31}\text{P}$  NMR chemical shifts to 85%  $\text{H}_3\text{PO}_4$ . Elemental analyses (C, H and N) were performed with a Vario EIII Chnso instrument. Electrochemical measurements were conducted with a CHI 660C potentiostat. A single-compartment electrochemical cell contained a pre-polished platinum disk working electrode ( $d = 0.5$  mm), a platinum wire counter electrode, and a silver wire pseudo-reference electrode. Spectroelectrochemical experiments at room temperature were performed with an airtight optically transparent thin-layer electrochemical (OTTLE) cell (optical path length of ca. 200  $\mu\text{m}$ ) equipped with a Pt minigrid working electrode and  $\text{CaF}_2$  windows [46]. The cell was positioned

in the sample compartment of a Bruker Tensor FT-IR spectrometer (1 cm<sup>-1</sup> spectral resolution, 8 scans) or a Shimadzu UV-3600 UV-vis-NIR spectrophotometer. The controlled-potential electrolyses were carried out with a CHI 660C potentiostat. Dry CH<sub>2</sub>Cl<sub>2</sub> deaerated by bubbling with argon for 10 min was used to prepare solutions of 10<sup>-3</sup> M complexes and 10<sup>-1</sup> M n-Bu<sub>4</sub>NPF<sub>6</sub> (dry, recrystallized) added as the supporting electrolyte.

Density functional theory (DFT) calculations were performed using the Gaussian09 software [47] at the B3LYP/6-31G\* [48] levels of theory. The basis set employed was 6-31G\* (LanI2DZ for Ru atom). Geometry optimization was performed without any symmetry constraints. Electronic transitions were calculated by the time-dependent DFT (TD-DFT) method. The solvation effects in dichloromethane are included for part of the calculations with the conductor-like polarizable continuum model (CPCM) [49, 50].

## 2.2. Syntheses

### 2.2.1. Syntheses of 3b

KOH (2.8 g, 50 mmol) and CuI (0.1 g, 0.5 mmol) were added to a stirred toluene solution of *p*-iodoaniline (2.92 g, 12.5 mmol), *p*-bromoaniline **3a** (0.09 g, 0.50 mmol) and 1,10-phenanthroline (18 mg, 0.1 mmol) under an argon atmosphere. The mixture was stirred at 125 °C for 12 h. Chromatography on silica gel (CH<sub>2</sub>Cl<sub>2</sub>/petroleum ether 1/1) gave **3e** as a light-yellow powder. Yield: 1.27 g, 66%. <sup>1</sup>H NMR (500 MHz, CDCl<sub>3</sub>), δ (ppm): 3.79 (s, 6H, OMe), 6.79 (d, *J*(HH)=10.0 Hz, 2H), 6.81 (t, *J*(HH)=5.0 Hz, 2H), 6.83 (t, *J*(HH)=5.0 Hz, 2H), 7.03 (d, *J*(HH)=10.0 Hz, 4H), 7.24 (t, *J*(HH) = 10.0 Hz, 2H).

### 2.2.2. Syntheses of 3c

Trimethylsilylacetylene (0.92 mL, 6.58 mmol) was added to a stirred solution of **3b** (768 mg, 2.00 mmol), CuI (38 mg, 0.19 mmol), and [Pd(PPh<sub>3</sub>)<sub>4</sub>] (232 mg, 0.21 mmol) in Et<sub>3</sub>N (5 mL) and THF (15 mL) under an argon atmosphere, and the mixture was heated to reflux for 24 h. The solution was then cooled and filtered through a bed of Celite. The filtrate was evaporated under reduced pressure and purified by silica gel column chromatography (CH<sub>2</sub>Cl<sub>2</sub>/petroleum ether 1/2) to give **3c** as a light-yellow oil. Yield: 482 mg, 60%. <sup>1</sup>H NMR (500 MHz, CDCl<sub>3</sub>), δ (ppm): 0.24 (s, 9H, SiMe<sub>3</sub>), 3.79 (s, 6H), 6.80 (d, *J*(HH)=5.0 Hz, 2H), 6.82 (t, *J*(HH)=5.0 Hz, 2H), 6.86 (d, *J*(HH)=5.0 Hz, 2H), 7.05 (d, *J*(HH)=10.0 Hz, 2H), 7.27 (dd, *J*(HH)=10.0 Hz, 2H).

### 2.2.3. Syntheses of 3 [51]

A solution of [RuCp\*Cl(dppe)] (202 mg, 0.30 mmol), **3c** (100 mg, 0.25 mmol), and KF (116 mg, 2.00 mmol) in 20 mL CH<sub>3</sub>OH and 4 mL THF was heated to reflux under nitrogen atmosphere for 24 h. The crude product was collected by filtration and washed with methanol and hexane. The solid was dissolved in dichloromethane, precipitated by slow diffusion of hexane, then filtered and dried to give **3** as a yellow-needled crystal. Yield: 150 mg, 60%. <sup>1</sup>H NMR (500 MHz, CDCl<sub>3</sub>), δ (ppm): 1.55 (s, 15H, CH<sub>3</sub>), 2.05 (br, 2H), 2.68 (br, 2H), 3.77 (s, 6H), 6.66 (dd, *J*(HH)=10.0 Hz, 4H), 6.77 (d, *J*(HH)=10.0 Hz, 4H), 6.98 (dd, *J*(HH)=10.0 Hz, 4H), 7.19–7.33 (m, 16H, dppe-Ph and Ar), 7.79 (s, 4H).

$^{13}\text{C}$  NMR (125 MHz,  $\text{CDCl}_3$ ),  $\delta$  (ppm): 10.10 ( $\text{CH}_3$ ), 29.47 ( $\text{CH}_2$ ), 55.53 ( $\text{OCH}_3$ ), 92.46 ( $\text{C}_5\text{H}_5$ ), 114.43, 121.90, 125.50, 127.17, 127.21, 127.41, 127.45, 128.84, 130.77, 133.24, 133.84, 133.88, 141.80, 154.98.  $^{31}\text{P}$  NMR (200 MHz,  $\text{CDCl}_3$ ),  $\delta$  (ppm): 80.94. Anal. Calcd for  $\text{C}_{61}\text{H}_{66}\text{NO}_2\text{P}_2\text{Ru}$ : C, 72.67; H, 6.60. Found: C, 72.80; H, 6.57.

### 2.3. Crystallographic analysis

Single-crystals of **3** suitable for X-ray analysis were grown by slow diffusion of hexane into a solution of dichloromethane. A crystal with approximate dimensions of  $0.24 \times 0.23 \times 0.21 \text{ mm}^3$  was mounted on a glass fiber for diffraction experiments. Intensity data were collected on a Bruker APEX-IICCD diffractometer with Mo  $\text{K}\alpha$  radiation ( $0.71073 \text{ \AA}$ ) at room temperature (298 K). The structure was solved by a combination of direct methods (SHELXS-97) [52] and Fourier difference techniques and refined by full-matrix least squares (SHELXL-97) [53]. All non-H atoms were refined anisotropically. The hydrogens were placed in ideal positions and refined as riding atoms. Further crystal data and details of the data collection are summarized in Table S1 (Supplementary material). Selected bond distances and angles are given in Table 1.

The crystal of **3** suitable for X-ray crystallographic analysis was obtained from  $\text{CH}_2\text{Cl}_2/\text{hexane}$ . The molecular structure of **3** is shown in Figure 2. Details of data collection and refinement are presented in Table S1 (Supplementary material). Selected bond lengths and angles from single-crystal X-ray diffraction experiments for **3** are summarized in Table 1, with relevant data from DFT structural optimizations experiments of  $\mathbf{3}^{n+}$  ( $n=0, 1, 2$ ) for comparison. As shown in the molecular structure of **3** (Figure 3), the  $\text{Ru}(\text{dppe})\text{Cp}^*$  terminal group had a similar pseudo-octahedral geometry. The two Ru-P bond distances were 2.250 and 2.2256  $\text{\AA}$ . Along the phenyl ethynyl bridge chain between  $\text{Ru}(\text{dppe})\text{Cp}^*$  and  $\text{NAr}_2$ , the Ru(1)-C(37), C(37)-C(38), C(38)-C(39), and C(42)-N(1) distances were 2.003, 1.208, 1.440, and 1.424  $\text{\AA}$ , respectively. The bond

**Table 1.** Selected bond lengths ( $\text{\AA}$ ) and angles (deg) from crystal structure of **3** and the full DFT-optimized structures  $\mathbf{3}^{n+}$  ( $n=0, 1, 2$ ).

	$\mathbf{3}_{\text{exp}}$	$\mathbf{3}_{\text{cal}}$	$\mathbf{3}^+$	$\mathbf{3}^{2+}$
Ru(1)-C(37)	2.003	2.027	1.951	1.902
Ru(1)-P(1, 2)	2.250, 2.256	2.335, 2.337	2.367, 2.382	2.383, 2.403
C(37)-C(38)	1.208	1.234	1.249	1.264
C(38)-C(39)	1.440	1.428	1.400	1.371
C(39)-C(40)	1.387	1.414	1.424	1.440
C(40)-C(41)	1.378	1.391	1.378	1.365
C(41)-C(42)	1.382	1.406	1.420	1.434
C(42)-N(1)	1.424	1.419	1.387	1.364
N(1)-C(45)	1.410	1.423	1.433	1.430
N(1)-C(52)	1.408	1.423	1.433	1.430
C(45)-C(46)	1.373	1.407	1.399	1.402
C(46)-C(47)	1.382	1.389	1.396	1.391
C(47)-C(48)	1.375	1.403	1.402	1.405
C(48)-O(1)	1.368	1.367	1.360	1.349
O(1)-C(51)	1.396	1.423	1.426	1.431
P(1)-Ru(1)-P(2)	83.23	83.58	82.76	82.28
Ru(1)-C(37)-C(38)	176.99	176.29	175.69	174.78
C(37)-C(38)-C(39)	176.87	178.94	179.50	179.83
C(42)-N(1)-C(45)	120.67	120.11	121.33	117.20
Ru ... N distance	8.879	8.963	8.840	8.740

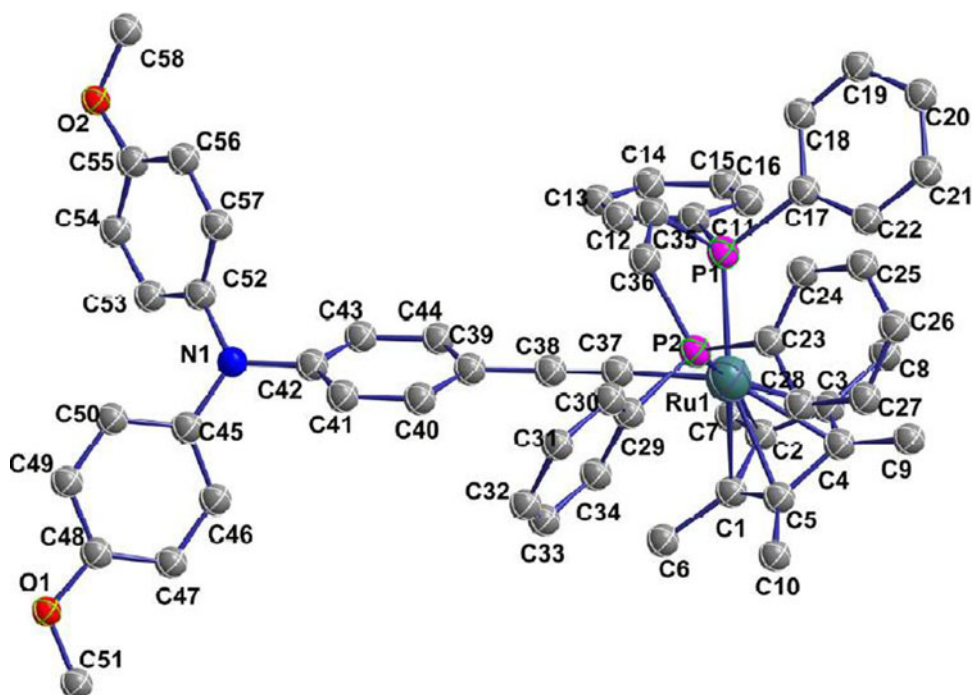


**Figure 2.** Molecular structure of **3** showing the selected atom labeling scheme. Hydrogens have been removed for clarity.

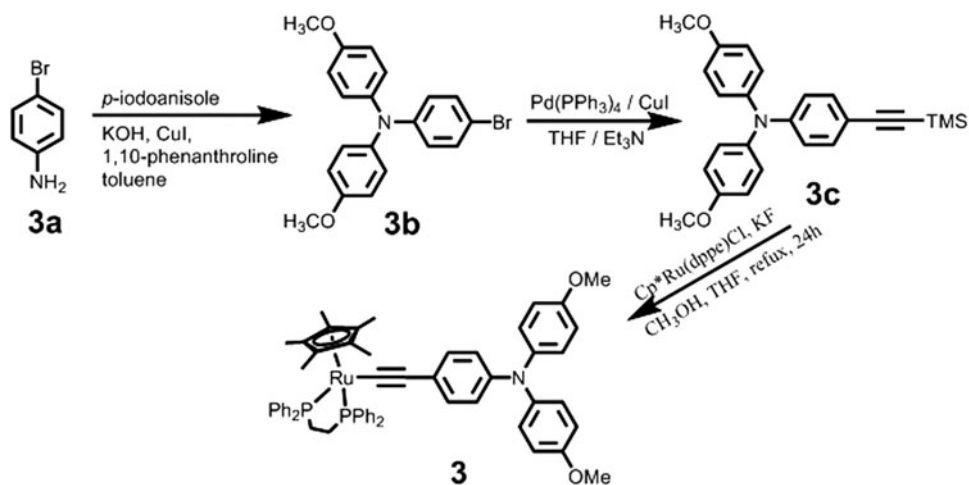


**Figure 3.** Synthetic routes to triarylamine-ethynyl ruthenium complex **3**.

lengths of the geometry-optimized structure **3** are in good agreement with those of the crystal structure, with a difference of about 0.02 Å. As the optimized structure was from the neutral state **3** to monocation **3**<sup>+</sup> and to dication **3**<sup>2+</sup>, the Ru(1)-C(37), C(42)-N(1) bond lengths and the distance between Ru(dppe)Cp\* and NAr<sub>2</sub> were gradually shortened and the C(37)-C(38) triple bond length was extended.

### 3. Results and discussion

#### 3.1. Syntheses and characterization

Target complex **3** was synthesized with 60% yield via three steps using classical C-N coupling reaction between 4-bromoaniline and *p*-iodoanisole, as well as Pd/Cu-catalyzed Sonogashira coupling reaction between **3b** and trimethylsilylacetylene. Subsequently, the TMS-protected compound **3c** was deprotected with KF and reacted *in situ* with [RuCl(dppe)Cp\*] at 60 °C. The general synthesis route to prepare **3** is shown in Figure 3. Target complex **3** was obtained by filtration and characterized by conventional spectroscopic methods. The nuclear magnetic resonance (NMR) spectrum of compound **3** showed the characteristic proton signals of **3** in the <sup>1</sup>H NMR spectrum at 1.55 ppm (CH<sub>3</sub>), 2.05 and 2.68 ppm (CH<sub>2</sub>), and 3.77 ppm (OCH<sub>3</sub>). The corresponding characteristic carbon spectrum signals appeared at 10.10 ppm (CH<sub>3</sub>), 29.47 ppm (CH<sub>2</sub>), 55.53 ppm (OCH<sub>3</sub>), and 92.46 ppm (C<sub>5</sub>H<sub>5</sub>), respectively. The <sup>31</sup>P NMR resonance of **3** always remained at around 80 ppm. The above characteristic signal peaks were consistent with those previously reported for ruthenium-ethynyl compounds [51].

#### 3.2. Electrochemical properties

The electrochemical properties of the bromotriarylamine precursor **3b** and complex **3** were investigated by cyclic voltammetry (CV) and square-wave voltammetry (SWV) in the CH<sub>2</sub>Cl<sub>2</sub>/n-Bu<sub>4</sub>NPF<sub>6</sub> supporting electrolyte. The CV and SWV combined curves are presented in Figure 4. Relevant electrochemical data were collected and are shown in Table 2, along with those for reported complexes **1** and **2**. Precursor **3b** exhibited a typical oxidation wave based on triarylamine at 0.76 V versus Fc<sup>0/+</sup> and an irreversible redox peak appeared at around 1.5 V versus Fc<sup>0/+</sup>, which can be originated from the second oxidation of triarylamine [43, 54]. The electrochemical diagram of the asymmetric redox-active complex **3** reported in this work showed that it had undergone two well-defined single-electron redox processes. The first (*E*<sub>1/2</sub>(1)) and second (*E*<sub>1/2</sub>(1)) half-wave potentials were at 0.16 and 0.66 V versus Fc<sup>0/+</sup>, and the latter was closer to the oxidation potential of the precursor molecule **3b**, corresponding to the

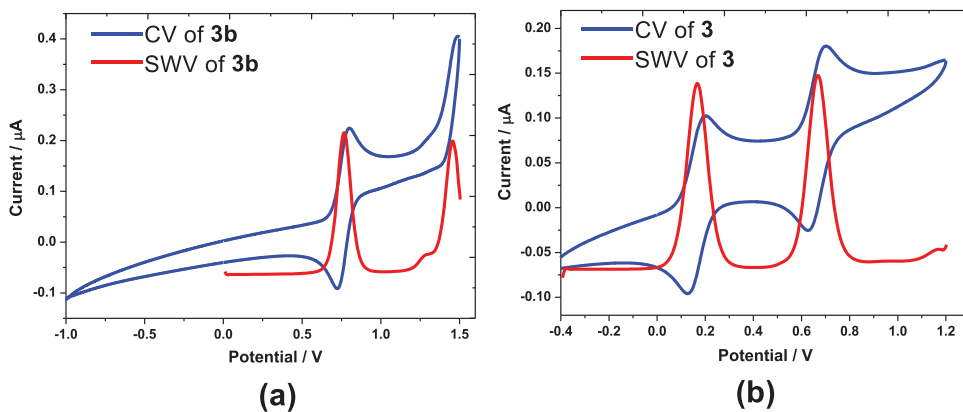


**Figure 4.** Cyclic voltammograms (CV) (blue line) at 0.1 V s<sup>-1</sup> and square-wave voltammograms (SWV) (red line) at 0.1 V s<sup>-1</sup>, *f* = 10 Hz of (a) **3b** and (b) **3** in CH<sub>2</sub>Cl<sub>2</sub>/n-Bu<sub>4</sub>NPF<sub>6</sub>.

electrochemical behaviors of ruthenium and triphenylamine, respectively. This result indicated that the Ru<sup>II/III</sup> process occurred prior to the N<sup>0/+</sup> process, which was also further supported by spin-density distribution calculations. The  $\Delta E_{1/2}$  and  $K_c$  values are often used to evaluate the degree of charge delocalization and the stability of MV states. The  $\Delta E_{1/2}$  values of **1–3** were 390, 410, and 500 mV, respectively. The difference in  $\Delta E_{1/2}$  may result from changes in the redox-active terminal groups, Ru-N distance and experimental conditions [55], which cannot be used as a comparison parameter for the charge delocalization and MV state stability of **1–3**. To further explore the electronic coupling of **3**, *in situ* spectroelectrochemical methods and DFT calculations were needed to analyze the distribution of charge and spin density in the oxidized forms, as reflected in the following studies.

### 3.3. IR spectroelectrochemical studies

Monitoring IR spectroscopic  $\nu(\text{C}\equiv\text{C})$  changes through electrolytic oxidation experiments by using air-tight spectroelectrochemical cells fitted with CaF<sub>2</sub> windows can provide deep insights into the electronic properties of MV state [56]. Accordingly, the

**Table 2.** Electrochemical data for **3b** and **3<sup>a</sup>** and reference complexes **1** and **2**.

Compound	$E_{1/2}(1)$ (V)	$E_{1/2}(2)$ (V)	$\Delta E_{1/2}$ (mV) <sup>b</sup>	$K_c$ <sup>e</sup>
<b>3b</b>	0.76	–	–	–
<b>3</b>	0.16	0.66	500	$2.83 \times 10^8$
<b>1<sup>c</sup></b>	–0.12	0.27	390	$3.91 \times 10^6$
<b>2<sup>d</sup></b>	0.27	0.68	410	$8.52 \times 10^6$

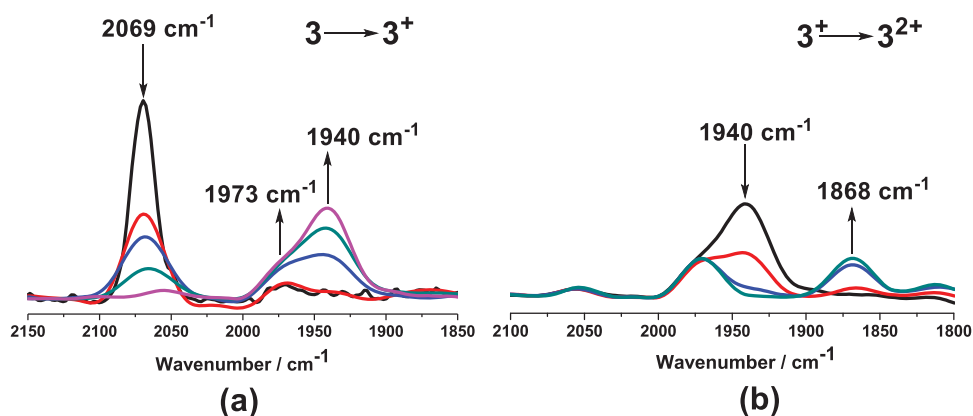
<sup>a</sup>Potential data in volts vs. Fc<sup>+</sup>/Fc are from single scan cyclic voltammograms recorded at 298 K in 0.1 M dichloromethane solution of n-Bu<sub>4</sub>NPF<sub>6</sub>. Potential is provided against the internal Cp<sub>2</sub>Fe<sup>0/+</sup> standard ( $E_{1/2} = 0.21$  V). Additional oxidation waves of triphenylamine observed at higher potentials (above 1.0 V) but not analyzed further.

<sup>b</sup> $\Delta E_{1/2} = E_{1/2}(2) - E_{1/2}(1)$  denotes the potential difference between two redox processes.

<sup>c</sup>See ref. [18c], and potential is provided against the internal Cp<sub>2</sub>Fe<sup>0/+</sup> standard ( $E_{1/2} = 0.000$  V).

<sup>d</sup>See ref. [18d], and potential is provided against the internal Cp<sub>2</sub>Fe<sup>0/+</sup> standard ( $E_{1/2} = 0.45$  V).

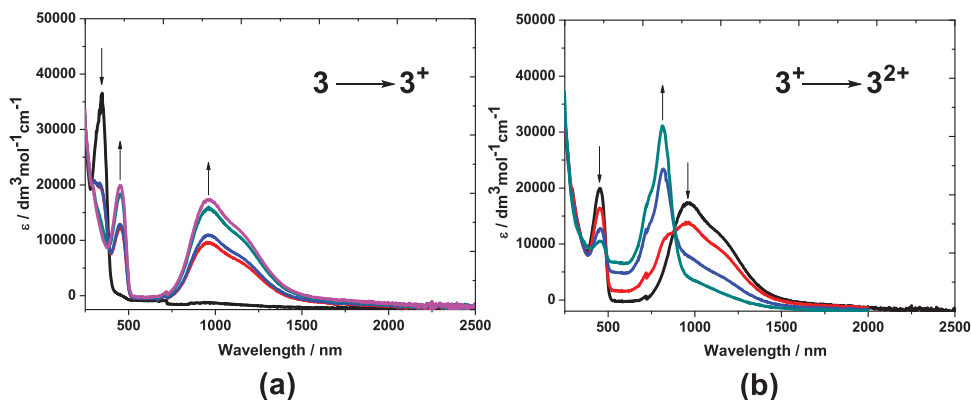
<sup>e</sup>The comproportionation constants,  $K_c$ , were calculated by the formula  $K_c = \exp(\Delta E_{1/2}/25.69)$  at 298 K.



**Figure 5.** IR spectroscopic changes in the  $\nu(\text{C}\equiv\text{C})$  region during the (a) first and (b) second oxidations of **3** (CH<sub>2</sub>Cl<sub>2</sub>/0.1 M n-Bu<sub>4</sub>NPF<sub>6</sub>).

**Table 3.** IR  $\nu(\text{C}\equiv\text{C})$  Spectra data recorded for rutheniumethynyl – TAA complex  $3^{n+}$  ( $n = 0, 1, 2$ )<sup>a</sup>.

Complex	$\nu(\text{C}\equiv\text{C})_{\text{exp}}$
<b>3</b>	2069 $\text{cm}^{-1}$
<b>3<sup>+</sup></b>	1973 $\text{cm}^{-1}$ , 1940 $\text{cm}^{-1}$
<b>3<sup>2+</sup></b>	1973 $\text{cm}^{-1}$ , 1868 $\text{cm}^{-1}$

<sup>a</sup>In  $\text{CH}_2\text{Cl}_2/\text{n-Bu}_4\text{NPF}_6$  (0.1 M) at room temperature.**Figure 6.** UV-vis-NIR spectral changes recorded during the oxidation (a)  $3 \rightarrow 3^+$  and (b)  $3^+ \rightarrow 3^{2+}$  in  $\text{CH}_2\text{Cl}_2/10^{-1}$  M  $\text{n-Bu}_4\text{NPF}_6$  at 298 K within a OTTLE cell.

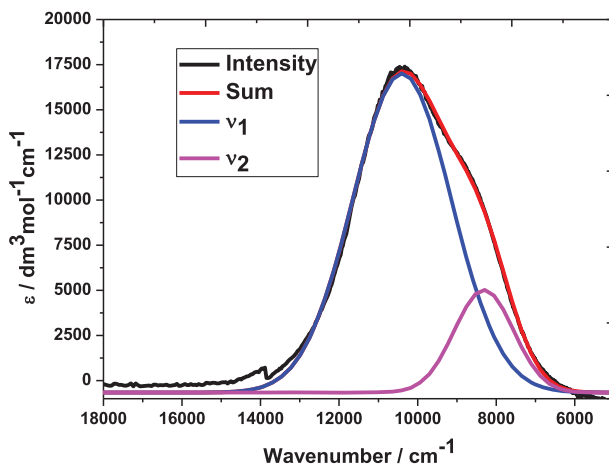
IR spectroelectrochemistry of **3** was studied. IR spectroscopic changes during one- and two-electron oxidation processes in the  $\nu(\text{C}\equiv\text{C})$  region are displayed in Figure 5. Pertinent  $\nu(\text{C}\equiv\text{C})$  data from experiments and DFT calculations are listed in Table 3. Upon the one-electron oxidation of **3**, the intensity of the characteristic  $\nu(\text{C}\equiv\text{C})$  band at 2069  $\text{cm}^{-1}$  decreased and was replaced by a new intense band at 1940  $\text{cm}^{-1}$  along with a weak shoulder peak at 1973  $\text{cm}^{-1}$ . The  $\nu(\text{C}\equiv\text{C})$  band shifted by 129  $\text{cm}^{-1}$  from **3** to **3<sup>+</sup>**. Similar results have been obtained from previously reported monoruthenium acetylide complexes  $[\text{Ru}(\text{C}\equiv\text{CAr})(\text{dppe})\text{Cp}^*]$  (Ar = phenyl, p-methylphenyl, 1-naphthyl and 9-anthracene), with one-electron oxidation resulting in a shift of the  $\nu(\text{C}\equiv\text{C})$  band range from 116  $\text{cm}^{-1}$  to 145  $\text{cm}^{-1}$  [57]. These comparative results revealed the bond-character changes of the 18-electron ruthenium acetylide units and suggested that the hole or radical cation was largely delocalized over the ruthenium acetylide terminal.

### 3.4. UV/vis/NIR spectroelectrochemistry

To enable detailed investigation of the electronic-transfer process, UV-vis-NIR spectroelectrochemical studies were conducted on **3** through electrolysis experiments involving single and double oxidation within an OTTLE cell (Figure 6). The spectroscopic data of three valence states are listed in Table 4. The spectrum of the neutral molecule **3** was dominated by an intense band at 350 nm (28,570  $\text{cm}^{-1}$ ). Gradual oxidation of **3** to stable monocation **3<sup>+</sup>** resulted in the disappearance of UV absorption from neutral molecule **3**, which was accompanied by the appearance of an absorption

**Table 4.** UV/Vis/NIR spectroscopic data of **3** and its oxidation products in dichloromethane/*n*-Bu<sub>4</sub>NPF<sub>6</sub>.

Complex	$\nu_{\max}$ (nm) ( $\epsilon_{\max}$ (dm <sup>3</sup> mol <sup>-1</sup> cm <sup>-1</sup> ))
<b>3</b>	350 (36150)
<b>3<sup>+</sup></b>	453 (19900), 961 (17480)
<b>3<sup>2+</sup></b>	455(10480), 812 (30930)

**Figure 7.** Gaussian-fitting of the NIR transitions of **3<sup>+</sup>** in CH<sub>2</sub>Cl<sub>2</sub>. The blue curve is the IVCT band.

band in the visible region at 453 nm (22,075 cm<sup>-1</sup>) and a broad NIR absorption band at 961 nm (10,405 cm<sup>-1</sup>). The characteristic and rather intense band enabled further detection of the existence of stable radical cation **3<sup>+</sup>**, which was assigned to donor-to-acceptor charge-transfer transitions [38]. As the step-by oxidation to **3<sup>2+</sup>**, the NIR absorption generated by **3<sup>+</sup>** disappeared and a very intense peak at 812 nm (12315 cm<sup>-1</sup>) was found in the visible region, similar to the highly intense bands observed in previously reported triarylamine systems [37–41, 45]. Thus, the second oxidation process was based on the triarylamine redox-active terminal.

Generally, IVCT bands in the NIR spectrum area from MV systems can be discussed by virtue of Hush's theory [14, 15, 58, 59]. This theory allows the determination of the two most important electron-transfer parameters (the reorganization energy  $\lambda$  and the electronic coupling parameter  $H_{ab}$ ) from the IVCT band. The comparison of both parameters can also be used to classify the systems [2, 3]. Thus, to determine the class in which the MV complex **3<sup>+</sup>** belongs, the NIR spectrum of **3<sup>+</sup>** was deconvoluted into two groups of sub-bands ( $\nu_1$  and  $\nu_2$ ) (Figure 7). According to a previous report [38],  $\nu_1$  may be attributed to IVCT transition absorption. By analyzing  $\nu_1$ , the relevant parameters can be obtained with  $\nu_{\max} = 10,370$  cm<sup>-1</sup>,  $\Delta\nu_{1/2} = 2810$  cm<sup>-1</sup>, and  $\epsilon_{\max} = 16,920$  M<sup>-1</sup> cm<sup>-1</sup>. According to the Hush formula [60, 61]  $H_{ab} = 2.06 \times 10^{-2} (\epsilon_{\max} \nu_{\max} \Delta\nu_{1/2})^{1/2} / (r_{ab})$ , where  $r_{ab}$  is the linear distance between metal ruthenium and nitrogen atoms in the crystal structure (8.879 Å), the electronic coupling parameter  $H_{ab}$  in CH<sub>2</sub>Cl<sub>2</sub> can roughly be figured out to be 1629 cm<sup>-1</sup>. The calculated  $H_{ab}$  was significantly lower than  $\nu_{\max}/2$  (5185 cm<sup>-1</sup>), demonstrating that MV complex **3<sup>+</sup>** may be classified as a class II MV system. However,  $H_{ab}$  may be usually underestimated in

strong electronic coupling systems owing to the shortened distance among redox-active end groups.

### 3.5. DFT and TD-DFT calculations

To further probe the electronic structure and the nature of frontier molecular orbitals of  $\mathbf{3}^{n+}$  ( $n=0, 1, 2$ ), we performed DFT (TD-DFT) calculations for  $\mathbf{3}^{n+}$  ( $n=0, 1, 2$ ) on the level of UB3LYP/6-31G\* theory (6-31G\* (Lan12DZ for the Ru atom)). Solvent effects were considered based on the conductor polarizable continuum model (CPCM) in  $\text{CH}_2\text{Cl}_2$  (see details in the Experimental section). Selected frontier molecular orbitals from  $\mathbf{3}^{n+}$  ( $n=0, 1, 2$ ) are displayed in Figure 8. The spin-density distribution with Mulliken segmental analysis of  $\mathbf{3}^+$  and  $\mathbf{3}^{2+}$  (double charges, triplet) is shown in Figure 9.

The highest occupied molecular orbital (HOMO) of neutral state  $\mathbf{3}$  was fully delocalized over the entire molecular skeleton (ruthenium ethynyl and TAA fragment), and HOMO-1 was strongly dominated by the ruthenium-alkynyl unit. Conversely, the LUMO and LUMO + 1 were generally localized on the ruthenium end group and exhibited an obvious metal character. To calculate the singly oxidized state  $\mathbf{3}^+$  and a doubly oxidized state  $\mathbf{3}^{2+}$ , the  $\beta$ -LUSO of  $\mathbf{3}^+$  and HOMO of  $\mathbf{3}^{2+}$  were mainly associated with the ruthenium-ethynyl and phenyl bridge, but the latter had a larger contribution from the TAA terminal. The visual spin-density distribution and Mulliken segmental analysis of  $\mathbf{3}^+$  (Figure 9(a)) revealed that the spin density was delocalized over the entire molecule skeleton and mainly resided on the ruthenium ethynyl terminal, which in combination with the IR spectroscopy data implied a possible

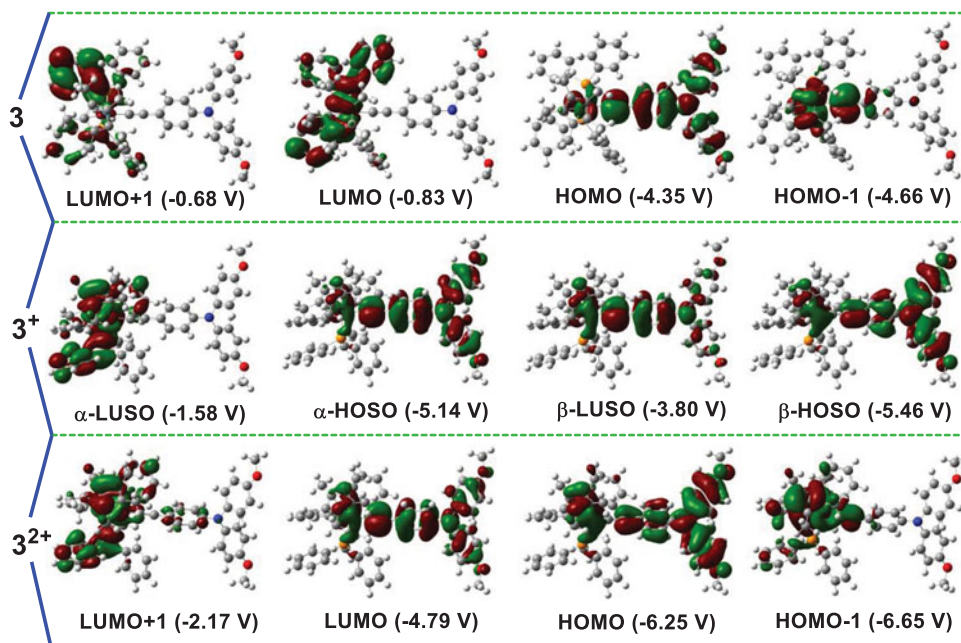


**Figure 8.** Selected frontier molecular orbitals from  $\mathbf{3}^{n+}$  ( $n=0, 1, 2$ ) plotted with contour values  $\pm 0.04$  ( $\text{e}/\text{bohr}^{3/2}$ ). B3LYP/6-31G\*(Ru: Lan12DZ)/CPCM/ $\text{CH}_2\text{Cl}_2$ .

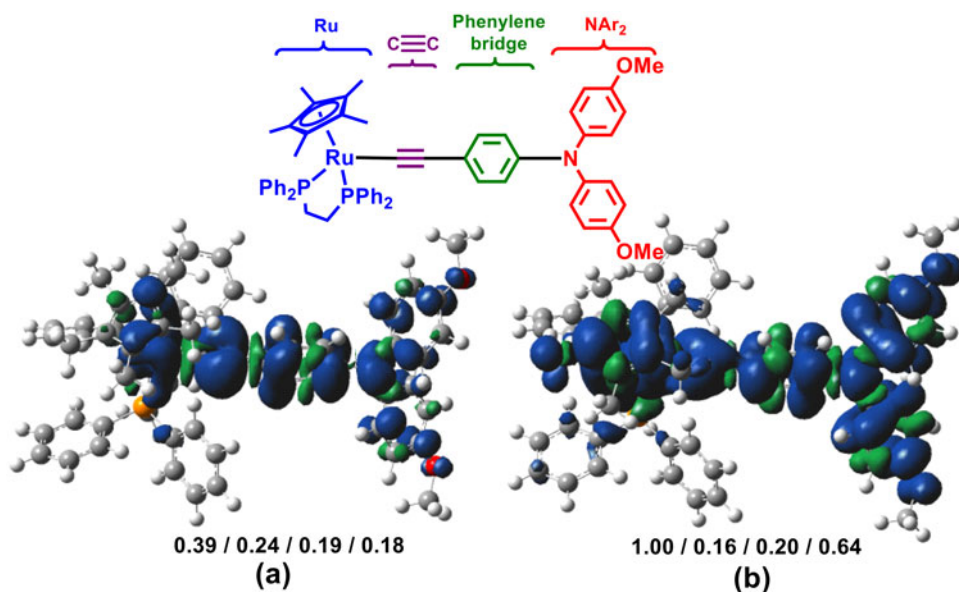


**Figure 9.** Calculated spin density distribution of (a)  $3^+$  and (b)  $3^{2+}$  (double charges, triplet) with fragment decomposition scheme (Ru/ $C\equiv C$ /Phenylene/ $NAr_2$ ). Contour values:  $\pm 0.04$  ( $e/\text{bohr}^3$ ) $^{1/2}$ . B3LYP/6-31G\*(Ru: LanI2DZ)/CPCM/ $CH_2Cl_2$ .

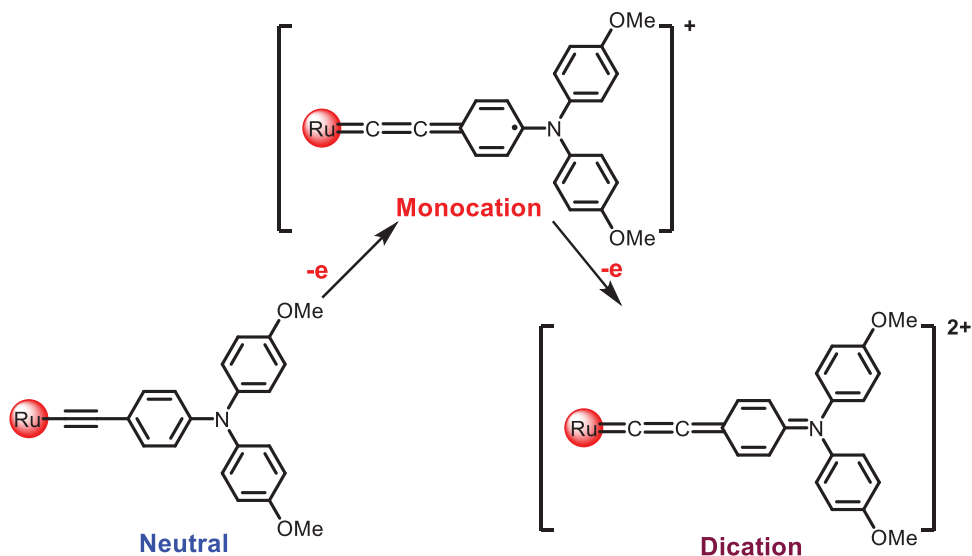


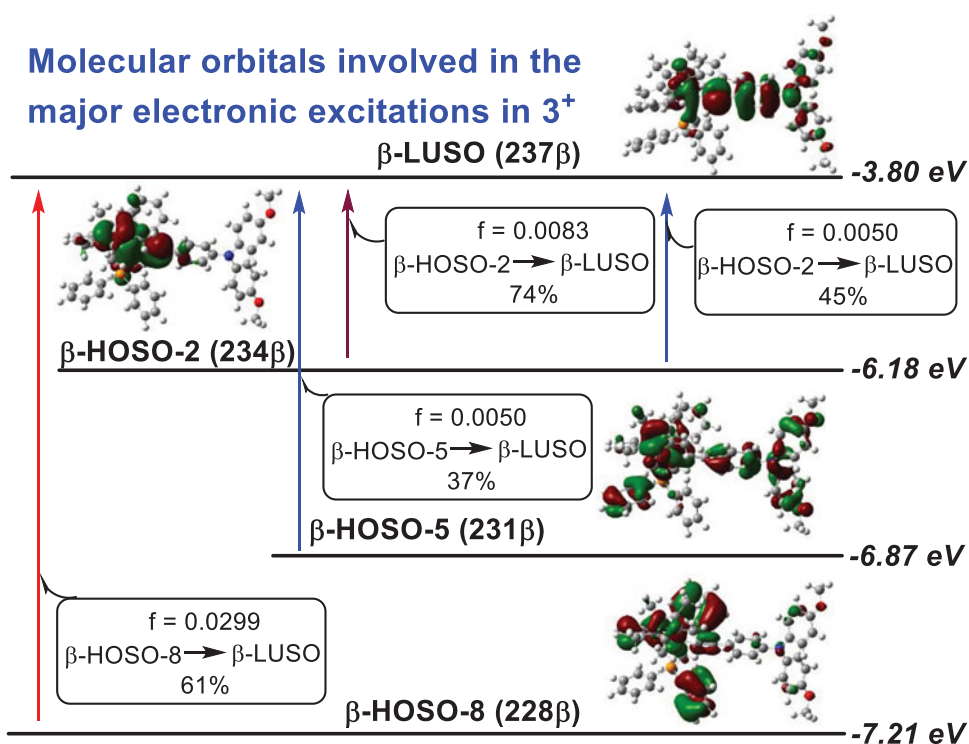
**Figure 10.** Structure change upon one-electronic and double-electron oxidation from electrolysis experiment.

structure change from a neutral to a singly oxidized state and to doubly oxidized state in **3** (Figure 10). The above calculated results all featured a ruthenium-dominated initial oxidation step and were consistent with the electrochemical findings. Moreover, the calculated distribution of spin density in the asymmetric double-oxidized state  $3^{2+}$  (Figure 9(b)) in their lowest energy triplet ground state also further suggested

**Table 5.** Major electronic excitations for  $3^{n+}$  ( $n = 0, 1, 2$ ) determined by TD-DFT methods (B3LYP/6-31G\*(Ru: LanI2DZ)/CPCM/CH<sub>2</sub>Cl<sub>2</sub>).

Species	Energy (cm <sup>-1</sup> )	$\lambda$ (nm)	$f$	Major contribs	Assignment
<b>3</b>	27070	369.4	0.1655	HOMO→LUMO + 1 (47%)	ILCT
	28290	353.5	0.6532	HOMO→LUMO + 4 (54%)	Ru→dppe CT/ILCT
<b>3<sup>+</sup></b>	10400	961.8	0.0050	$\beta$ -HOSO-5→ $\beta$ -LUSO (37%) $\beta$ -HOSO-2→ $\beta$ -LUSO (45%)	NAr <sub>2</sub> →Ru CT/Ru-C≡C→Phenyl bridge CT
	10990	909.8	0.0083	$\beta$ -HOSO-2→ $\beta$ -LUSO (74%)	Ru-C≡C→Phenyl bridge CT
	14470	691.0	0.0299	$\beta$ -HOSO-8→ $\beta$ -LUSO (61%)	dppe and Cp* to Ru CT mixed with ILCT
<b>3<sup>2+</sup></b>	12305	812.7	0.2725	HOMO-5→LUMO (67%)	dppe to Ru CT mixed with ILCT

### Molecular orbitals involved in the major electronic excitations in 3<sup>+</sup>

**Figure 11.** Isosurface plots of molecular orbitals involved in the major electronic excitations for  $3^+$ .

sequential Ru<sup>II/III</sup> and An<sub>3</sub>N<sup>0/+</sup> oxidation processes. The second oxidation step was proved by characteristic N<sup>•+</sup>-localized transition absorption [39–41] through UV-vis-NIR spectroelectrochemical experiments.

To assign the related absorptions of  $3^{n+}$  ( $n = 0, 1, 2$ ) and understand their transition features, TD-DFT calculations were performed on the above DFT-optimized structure based on CPCM in CH<sub>2</sub>Cl<sub>2</sub>. According to TDDFT predictions and transitions assignments (Table 5), the absorptions from  $3^{n+}$  ( $n = 0, 1, 2$ ) agreed with the experimental spectroscopy results. Accordingly, selected frontier orbitals involved in the transitions

for  $\mathbf{3}^{n+}$  ( $n=0, 1, 2$ ) are shown in Figures 11 and S1–S2 (Supplementary material). The absorption of the neutral molecule  $\mathbf{3}$  was at 350 nm from UV experimental data, and this absorption was better assigned to Ru→dppe CT/ILCT and featured major contributions of HOMO→LUMO + 4 (353.5 nm (28 290 cm<sup>-1</sup>) with oscillator strength  $f=0.6532$ ). The experimental NIR absorption of monocation  $\mathbf{3}^+$  was correctly predicted by TD-DFT calculations exhibiting low-energy transition at 961.8 nm (10,400 cm<sup>-1</sup> with  $f=0.0050$ ), which featured  $\beta$ -HOSO-5→ $\beta$ -LUSO and  $\beta$ -HOSO-2→ $\beta$ -LUSO transitions. This finding revealed NAr<sub>2</sub>→Ru charge transfer mixed with Ru-C≡C→phenyl bridge charge-transfer. Finally, TDDFT results of  $\mathbf{3}^{2+}$  suggested that the intense absorption at 812 nm (30,930 cm<sup>-1</sup>) was generated by HOMO-5→LUMO transition (Supplementary material, Figure S2), which exhibited the dppe to Ru charge transfer transition and TAA<sup>+</sup> intraligand absorption ILCT characters.

## 4. Conclusion

A novel organic-inorganic hybrid MV system model  $\mathbf{3}$  was established and characterized by X-ray single-crystal diffraction and molecular spectroscopy techniques. The electronic properties of different valence states  $\mathbf{3}^{n+}$  ( $n=0, 1, 2$ ) were investigated by electrochemistry through *in situ* IR and UV-vis-NIR spectroelectrochemical methods combined with DFT (TD-DFT) calculations. Comparative electrochemical results revealed that the first one-electron oxidation process occurred in the RuCp\*(dppe) fragment, which was also supported further by large  $\nu(\text{C}\equiv\text{C})$  band shifts (129 cm<sup>-1</sup>) from  $\mathbf{3}$  to  $\mathbf{3}^+$  and spin-density distribution calculations of monocation  $\mathbf{3}^+$ . The characteristic and rather intense NIR absorption band of  $\mathbf{3}^+$  was found in UV-vis-NIR spectra, and relevant parameters were analyzed by Hush theory and subsequently classified  $\mathbf{3}^+$  as a Class II MV system, which may be underestimated due to the misjudgment of Ru-N distance. The absorptions from  $\mathbf{3}^{n+}$  ( $n=0, 1, 2$ ) were better predicted by TD-DFT calculations and well agreed with those of experimental spectroscopy results. This work provided another supplement for the design and synthesis of a new type of organic-inorganic hybrid MV system.

## Disclosure statement

No potential conflict of interest was reported by the authors.

## Funding

The authors acknowledge the financial support from National Natural Science Foundation of China (21602049, 21472059, 21402057), the Natural Science Foundation of Hunan Province, China (No. 2017JJ3004), the Aid Programs for Technology Innovative Team and Key Discipline in Education Department of Hunan Province.

## References

- [1] M.M. Hansmann, M. Melaimi, G. Bertrand. *J. Am. Chem. Soc.*, **140**, 2206 (2018).
- [2] J. Hankache, O.S. Wenger. *Chem. Rev.*, **111**, 5138 (2011).

- [3] P. Aguirre-Etcheverry, D. O'Hare. *Chem. Rev.*, **110**, 4839 (2010).
- [4] Y.-P. Ou, C. Jiang, D. Wu, J. Xia, J. Yin, S. Jin, G.-A. Yu, S.H. Liu. *Organometallics*, **30**, 5763 (2011).
- [5] S. Roué, H. Sahnoune, L. Toupet, J.-F. Halet, C. Lapinte. *Organometallics*, **35**, 2057 (2016).
- [6] H.W. Chen, S. Mallick, S.F. Zou, M. Meng, C.Y. Liu. *Inorg. Chem.*, **57**, 7455 (2018).
- [7] A. Hildebrandt, H. Lang. *Organometallics*, **32**, 5640 (2013).
- [8] D. Miesel, A. Hildebrandt, M. Korb, D. Schaarschmidt, H. Lang. *Organometallics*, **34**, 4293 (2015).
- [9] C.-J. Yao, Y.-W. Zhong, J. Yao. *J. Am. Chem. Soc.*, **133**, 15697 (2011).
- [10] Y.-P. Ou, J. Zhang, M.-X. Zhang, F. Zhang, D. Kuang, F. Hartl, S.H. Liu. *Inorg. Chem.*, **56**, 11074 (2017).
- [11] S.H. Liu, Q.Y. Hu, P. Xue, T.B. Wen, I.D. Williams, G. Jia. *Organometallics*, **24**, 769 (2005).
- [12] S. Scheerer, N. Rotthowe, O.S. Abdel-Rahman, X. He, S. Rigaut, H. Kvapilová, S. Zális, R.F. Winter. *Inorg. Chem.*, **54**, 3387 (2015).
- [13] C.E.B. Evans, M.L. Naklicki, A. Rezvani, C.A. White, V.V. Kondratiev, R.J. Crutchley. *J. Am. Chem. Soc.*, **120**, 13096 (1998).
- [14] D.M. D'Alessandro, F.R. Keene. *Chem. Soc. Rev.*, **35**, 424 (2006).
- [15] K.D. Demadis, C.M. Hartshorn, T.J. Meyer. *Chem. Rev.*, **101**, 2655 (2001).
- [16] G.-L. Xu, G. Zou, Y.-H. Ni, M.C. DeRosa, R.J. Crutchley, T. Ren. *J. Am. Chem. Soc.*, **125**, 10057 (2003).
- [17] H. Qi, A. Gupta, B.C. Noll, G.L. Snider, Y. Lu, C. Lent, T.P. Fehlner. *J. Am. Chem. Soc.*, **127**, 15218 (2005).
- [18] M.A. Fox, B.L. Guenic, R.L. Roberts, D.A. Brue, D.S. Yufit, J.A.K. Howard, G. Manca, J.-F. Halet, F. Hartl, P.J. Low. *J. Am. Chem. Soc.*, **133**, 18433 (2011).
- [19] J. Zhang, M.-X. Zhang, C.-F. Sun, M. Xu, F. Hartl, J. Yin, G.-A. Yu, L. Rao, S.H. Liu. *Organometallics*, **34**, 3967 (2015).
- [20] U. Pfaff, A. Hildebrandt, D. Schaarschmidt, T. Ruffer, P.J. Low, H. Lang. *Organometallics*, **32**, 6106 (2013).
- [21] R. Makhoul, Y. Kumamoto, A. Miyazaki, F. Justaud, F. Gendron, J.-F. Halet, J.-R. Hamon, C. Lapinte. *Eur. J. Inorg. Chem.*, **2014**, 3899 (2014).
- [22] Y.-W. Zhong, Z.-L. Gong, J.-Y. Shao, J. Yao. *Coord. Chem. Rev.*, **312**, 22 (2016).
- [23] W. Kaim, G.K. Lahiri. *Angew. Chem. Int. Ed.*, **46**, 1778 (2007).
- [24] T. Nagashima, T. Nakabayashi, T. Suzuki, K. Kanaizuka, H. Ozawa, Y.-W. Zhong, S. Masaoka, K. Sakai, M. Haga. *Organometallics*, **33**, 4893 (2014).
- [25] M. Uebe, T. Kazama, R. Kurata, D. Sakamaki, A. Ito. *Angew. Chem.*, **129**, 15918 (2017).
- [26] V. Coropceanu, M. Malagoli, J.M. André, J.L. Brédas. *J. Am. Chem. Soc.*, **124**, 10519 (2002).
- [27] A. Jana, M. Ishida, J.S. Park, S. Bähring, J.O. Jeppesen, J.L. Sessler. *Chem. Rev.*, **117**, 2641 (2017).
- [28] A. Cecon, S. Santi, L. Orian, A. Bisello. *Coord. Chem. Rev.*, **248**, 683 (2004).
- [29] N. Bellec, A. Vacher, F. Barrière, Z. Xu, T. Roisnel, D. Lorcy. *Inorg. Chem.*, **54**, 5013 (2015).
- [30] A. Vacher, F. Barrière, T. Roisnel, L. Piekara-Sady, D. Lorcy. *Organometallics*, **30**, 3570 (2011).
- [31] W. Polit, P. Mücke, E. Wuttke, T. Exner, R.F. Winter. *Organometallics*, **32**, 5461 (2013).
- [32] C. Sporer, I. Ratera, D. Ruiz-Molina, Y. Zhao, J. Vidal-Gancedo, K. Wurst, P. Jaitner, K. Clays, A. Persoons, C. Rovira, J. Veciana. *Angew. Chem. Int. Ed.*, **43**, 5266 (2004).
- [33] Z. Ning, H. Tian. *Chem. Commun.*, **37**, 5483 (2009).
- [34] J. Wang, K. Liu, L. Ma, X. Zhan. *Chem. Rev.*, **116**, 14675 (2016).
- [35] J. Schäfer, M. Holzapfel, B. Mladenova, D. Kattinig, I. Krummenacher, H. Braunschweig, G. Grampp, C. Lambert. *J. Am. Chem. Soc.*, **139**, 6200 (2017).
- [36] P.M. Burrezo, N.-T. Lin, K. Nakabayashi, S.-i. Ohkoshi, E.M. Calzado, P.G. Boj, M.A. Díaz García, C. Franco, C. Rovira, J. Veciana, M. Moos, C. Lambert, J.T. López Navarrete, H. Tsuji, E. Nakamura, J. Casado. *Angew. Chem. Int. Ed.*, **56**, 2898 (2017).
- [37] L. Chen, S. Mallick, Y.N. Tan, M. Meng, C.Y. Liu. *Inorg. Chem.*, **56**, 7470 (2017).
- [38] J.-H. Tang, S.-H. Wu, J.-Y. Shao, H.-J. Nie, Y.-W. Zhong. *Organometallics*, **32**, 4564 (2013).

- [39] C. Hassenrück, R.F. Winter. *Inorg. Chem.*, **56**, 13517 (2017).
- [40] C.-J. Yao, R.-H. Zheng, Q. Shi, Y.-W. Zhong, J. Yao. *Chem. Commun.*, **48**, 5680 (2012).
- [41] H.-J. Nie, J.-Y. Shao, C.-J. Yao, Y.-W. Zhong. *Chem. Commun.*, **50**, 10082 (2014).
- [42] M.-X. Zhang, J. Zhang, J. Yin, F. Hartl, S.H. Liu. *Dalton Trans.*, **47**, 6112 (2018).
- [43] E. Kovalski, M. Korb, A. Hildebrandt. *Eur. J. Inorg. Chem.*, **2018**, 671 (2018).
- [44] M.I. Bruce, B.G. Ellis, P.J. Low, B.W. Skelton, A.H. White. *Organometallics*, **22**, 3184 (2003).
- [45] C. Lambert, J. Schelter, T. Fiebig, D. Mank, A. Trifonov. *J. Am. Chem. Soc.*, **127**, 10600 (2005).
- [46] M. Krejčík, M. Daněk, F. Hartl. *J. Electroanal. Chem.*, **317**, 179 (1991).
- [47] M.J. Frisch, G.W. Trucks, H.B. Schlegel, G.E. Scuseria, M.A. Robb, J.R. Cheeseman, G. Scalmani, V. Barone, B. Mennucci, G.A. Petersson, H. Nakatsuji, M. Caricato, X. Li, H.P. Hratchian, A.F. Izmaylov, J. Bloino, G. Zheng, J.L. Sonnenberg, M. Hada, M. Ehara, K. Toyota, R. Fukuda, J. Hasegawa, M. Ishida, T. Nakajima, Y. Honda, O. Kitao, H. Nakai, T. Vreven, J.A. Montgomery, Jr., J.E. Peralta, F. Ogliaro, M. Bearpark, J.J. Heyd, E. Brothers, K.N. Kudin, V.N. Staroverov, R. Kobayashi, J. Normand, K. Raghavachari, A. Rendell, J.C. Burant, S.S. Iyengar, J. Tomasi, M. Cossi, N. Rega, J.M. Millam, M. Klene, J.E. Knox, J.B. Cross, V. Bakken, C. Adamo, J. Jaramillo, R. Gomperts, R.E. Stratmann, O. Yazyev, A.J. Austin, R. Cammi, C. Pomelli, J.W. Ochterski, R.L. Martin, K. Morokuma, V.G. Zakrzewski, G.A. Voth, P. Salvador, J.J. Dannenberg, S. Dapprich, A.D. Daniels, Ö. Farkas, J.B. Foresman, J.V. Ortiz, J. Cioslowski, D.J. Fox. *Gaussian 09, Revision D.01*, Gaussian, Inc., Wallingford, CT (2009).
- [48] T.H. Dunning. P.J. *Hay in Modern Theoretical Chemistry*, Vol. **3**, p. 1., H.F. Schaefer (Ed.), Plenum, New York (1976).
- [49] V. Barone, M. Cossi. *J. Phys. Chem. A*, **102**, 1995 (1998).
- [50] M. Cossi, N. Rega, G. Scalmani, V. Barone. *J. Comput. Chem.*, **24**, 669 (2003).
- [51] J. Xia, Y.-P. Ou, X.-G. Meng, J. Yin, G.-A. Yu, S.H. Liu. *Eur. J. Inorg. Chem.*, **2014**, 247 (2014).
- [52] G.M. Sheldrick. *SHELXS-97, A Program for Crystal Structure Solution*, University of Göttingen, Göttingen, Germany (1997).
- [53] G.M. Sheldrick. *SHELXL-97, A Program for Crystal Structure Refinement*, University of Göttingen, Göttingen, Germany (1997).
- [54] X. Zheng, X. Wang, Y. Qiu, Y. Li, C. Zhou, Y. Sui, Y. Li, J. Ma, X. Wang. *J. Am. Chem. Soc.*, **135**, 14912 (2013).
- [55] W.E. Geiger, F. Barrière. *Acc. Chem. Res.*, **43**, 1030 (2010).
- [56] M.A. Fox, J.D. Farmer, R.L. Roberts, M.G. Humphrey, P.J. Low. *Organometallics*, **28**, 5266 (2009).
- [57] M.A. Fox, R.L. Roberts, W.M. Khairul, F. Hartl, P.J. Low. *J. Organomet. Chem.*, **692**, 3277 (2007).
- [58] J.-P. Launay. *Chem. Soc. Rev.*, **30**, 386 (2001).
- [59] B.S. Brunshwig, C. Creutz, N. Sutin. *Chem. Soc. Rev.*, **31**, 168 (2002).
- [60] N.S. Hush. *Coord. Chem. Rev.*, **64**, 135 (1985).
- [61] N.S. Hush. *Prog. Inorg. Chem.*, **8**, 391(1967).